

# Planar potential flow on Cartesian grids

Diederik Beckers<sup>1</sup> and Jeff D. Eldredge<sup>1†</sup>

<sup>1</sup>Mechanical and Aerospace Engineering, University of California, Los Angeles, CA 90095-1597 USA

Potential flow has many applications, including the modelling of unsteady flows in aerodynamics. For these models to work efficiently, it is best to avoid Biot-Savart interactions between the potential flow elements. This work presents a grid-based solver for potential flows in two dimensions and its use in a vortex model for simulations of separated aerodynamic flows. The solver follows the vortex-in-cell approach and discretizes the streamfunction-vorticity Poisson equation on a staggered Cartesian grid. The lattice Green's function is used to efficiently solve the discrete Poisson equation with unbounded boundary conditions. In this work, we use several key tools that ensure the method works on arbitrary geometries, with and without sharp edges. The immersed boundary projection method is used to account for bodies in the flow and the resulting body forcing Lagrange multiplier is identified as a discrete version of the bound vortex sheet strength. Sharp edges are treated by decomposing the body-forcing Lagrange multiplier into a singular and smooth part. To enforce the Kutta condition, the smooth part can then be constrained to remove the singularity introduced by the sharp edge. The resulting constraints and Kelvin's circulation theorem each add Lagrange multipliers to the overall saddle point system. The accuracy of the solver is demonstrated in several problems, including a flat plate shedding singular vortex elements. The method shows excellent agreement with a Biot-Savart method when comparing the vortex element positions and the force.

## 1. Introduction

Potential flow plays an important role in aerodynamic modelling, but also appears in other areas such as the modelling of water waves or wind farms and added mass calculations. Besides its prominent use for steady flow around airfoils at high Reynolds numbers, potential flow theory has long provided the tools for vortex methods to simulate unsteady flows around airfoils and bluff bodies. These vortex methods discretize the vorticity in the flow with singular elements such as point vortices, vortex sheets, or a combination of both, and, in the case of an inviscid and incompressible model, the irrotational flow outside of these singular vortex elements is a potential flow. The singular vortex elements representing the free vorticity in an inviscid vortex model are tracked as Lagrangian points that are advected by the local flow velocity according to Helmholtz's second theorem. In case the vortex method inserts new vortex elements in the flow behind a bluff body or at sharp edges, Kelvin's circulation theorem dictates that the circulation should be conserved. Singular potential flow elements also serve to enforce the no-penetration condition, with the most common choice in vortex methods being a distribution of singular vorticity on the body, denoted as the bound vortex sheet. Besides their choice for the type of singular elements, potential flow solvers for vortex methods differ in their way of calculating the flow velocity. This can be done by either using direct interaction between the potential flow elements or by calculating the velocity on a grid over the entire domain and the eventual choice dictates the treatment of boundary and edge conditions.

In the first approach, the Green's function of the Laplacian is applied to the Poisson equation in the velocity-vorticity formulation to give the Biot-Savart integral, which provides the exact

† Email address for correspondence: [jdeldre@ucla.edu](mailto:jdeldre@ucla.edu)

solution for a velocity field that satisfies unbounded boundary conditions. Biot-Savart vortex methods often smooth the Biot-Savart kernel, equivalent to replacing point vortices by vortex blobs (Chorin & Bernard 1973), to suppress Kelvin-Helmholtz instabilities below a certain wavelength resulting from the interactions between closely spaced vortex elements. The solution generally requires  $O(N^2)$  operations, with  $N$  the number of vortex elements, to sum the influences of each discretized vortex element on every other element. With fast multipole methods, it scales optimally as  $O(N)$  but with a large prefactor and overhead cost. Inviscid vortex methods of this kind can straightforwardly use the potential flow tools to enforce the no-penetration, such as conformal mapping or solving the integral equation for a surface singularity distribution through analytical inversion, panel discretization, or with Fourier expansions. For a detailed review of this subject, the reader is referred to Cottet & Koumoutsakos (2000) and Eldredge (2019).

A second approach to calculate the flow velocity follows from the discretization of the Poisson equation in the velocity-vorticity formulation or streamfunction-vorticity formulation on a grid over the domain of interest and is called a vortex-in-cell (VIC) approach, first developed by Christiansen (1973). The procedure requires first to regularize the vorticity onto the grid, then to solve the discrete Poisson equation, and finally to interpolate the velocity (or curl of the streamfunction) to the Lagrangian vortex elements. It introduces discretization errors but only requires  $O(M \log M)$  operations, with  $M$  the number of grid points, to solve the Poisson equation with current numerical techniques and  $O(N)$  operations to perform the regularization and interpolation. Similar to the regularized Biot-Savart kernel, the grid spacing together with the vorticity regularization scheme determine the cut-off wavelength below which the Kelvin-Helmholtz instabilities get suppressed.

The early work on VIC methods focused on inviscid vortex dynamics using Fourier-based Poisson solvers with Dirichlet or periodic boundary conditions (Meng & Thomson 1978; Baker 1979; Couët *et al.* 1981) and the analysis of different interpolation kernels (Ebiana & Bartholomew 1996). After viscous schemes for vortex methods were introduced, VIC methods increasingly replaced Biot-Savart methods in an effort to speed up vortex methods for viscous flows, leading to methods with over a billion particles (Chatelain *et al.* 2008). This also stimulated the development of VIC methods for external flows over bodies, mostly for viscous flows. The most straightforward way to include a body in the flow is to use a body-fitted mesh as in Cottet & Poncet (2004), who apply the Helmholtz decomposition on the flow in their VIC method and place a Neumann boundary condition for the scalar potential on the body to account for its presence and employ an analytic boundary condition for the far-field. However, a body-fitted mesh is case-specific and, therefore, the same work (and later also Poncet (2009)), develops an immersed boundary method by introducing a singular distribution of sources that represents the influence of the body and is smeared onto a cartesian grid using a discrete approximation to the Dirac delta function. The result is a source term inserted in the Poisson equation for the scalar potential which is solved on the grid. Similar to the immersed boundary methods, Brinkman penalization methods do not require body-fitted meshes. In vortex methods, the Brinkman penalization method (Coquerelle & Cottet 2008; Rossinelli *et al.* 2010; Gazzola *et al.* 2011; Rasmussen *et al.* 2011; Chatelin & Poncet 2014) adds a volume forcing term to the vorticity transport equation that includes a penalization parameter, equivalent to the porosity of the body. However, the method suffers from a strong time step restriction, which motivated Hejlesen *et al.* (2015) to use an iterative Brinkman penalization method, which Spietz *et al.* (2017) extended to three dimensions.

The immersed boundary method and Brinkman penalization method both smear out the influence of the interface onto nearby grid points. LeVeque & Li (1994) developed the immersed interface method to overcome this issue and to obtain a higher spatial order of accuracy than the immersed boundary method. The premise of this method is to discretize the jump conditions caused by the interface with finite differences instead of discretizing the Dirac delta function, and the result is a sharp representation of the interface with a second or higher-order accuracy.

Marichal *et al.* (2014) applied the explicit-jump immersed interface method (Wiegmann & Bube 2000) in his potential flow method and condensed the influence of the interface in an extra source term in his streamfunction Poisson equation and recognizes that the term is equivalent to a bound vortex sheet strength regularized to the grid. He presents results from the flow over a cylinder and an airfoil, for which they discretized the Kutta condition on the grid with finite-differences. Gillis *et al.* (2018) extended the method to three dimensions but applies the immersed interface method on the scalar potential instead. He models the potential flow around a sphere and solves the Poisson equation using the lattice Green's function, which automatically takes care of the far-field boundary conditions.

The potential flow method that we propose in this present work is a VIC method on a Cartesian grid that uses point vortices to represent the bulk vorticity. We use the lattice Green's function to solve the streamfunction-vorticity Poisson equation with the immersed boundary projection method, which was initially developed for viscous flow by Colonius & Taira (2008). The corresponding Lagrange multiplier in the streamfunction Poisson equation is identified as the discrete analogue of the bound vortex sheet strength. This turns the attention to how the concept of the discrete vortex sheet strength can be leveraged to enforce the Kutta condition. Instead of discretizing a continuous version of the Kutta condition, we draw inspiration from the analytical treatment of the Kutta condition in Biot-Savart methods and eliminate the singularities from the discrete bound vortex sheet to ensure the flow velocity is bounded at a sharp edge. This is equivalent to constraining the algebraic system arising from the immersed boundary projection method to make the overall system well-behaved and can therefore be posed as a linear algebra problem. The result is a saddle point system that we solve with the Schur's complement method.

## 2. Methodology

### 2.1. The basic two-dimensional potential flow problem

We consider here a staggered, Cartesian grid with uniform cell size  $\Delta x$  and of infinite extent. The space corresponding to data at cell vertices (nodes) on this grid is denoted by  $\mathcal{N}$ , and the physical coordinates of these nodes by  $x$  and  $y$ . The basic (unbounded) potential flow problem is expressed as

$$\mathbf{L}s = -\mathbf{w}, \quad (2.1)$$

where  $\mathbf{L}$  is the discrete 5-point Laplacian operator,  $s \in \mathcal{N}$  is the discrete streamfunction, and  $\mathbf{w} \in \mathcal{N}$  the discrete vorticity. Following the vortex-in-cell approach (Christiansen 1973), the discrete vorticity is obtained by regularizing the vorticity from the  $N_v$  vortex elements onto the cell vertices,

$$\mathbf{w}_{i,j} = \sum_{q=1}^{N_v} \frac{1}{\Delta x} \Gamma_{v,q} d \left( \frac{x_i - X_q}{\Delta x} \right) d \left( \frac{y_j - Y_q}{\Delta x} \right), \quad (2.2)$$

where  $d$  is the  $M'_4$  interpolation kernel (Monaghan 1985), and  $(X_q, Y_q)$  and  $\Gamma_{v,q}$  are the position and strength of the  $q$ th vortex element.

The discrete velocity field  $\mathbf{v}$ , whose components lie on the faces of the cells with the corresponding normals, is computed from  $\mathbf{s}$  by the discrete curl operation,

$$\mathbf{v} = \mathbf{C}s. \quad (2.3)$$

The operator  $\mathbf{C}$  applies centered differences between the nodes to obtain the velocity components at the intermediate centers of cell faces. We denote the space of data that lie on cell faces by  $\mathcal{F}$ , so  $\mathbf{C} : \mathcal{N} \mapsto \mathcal{F}$ . After the velocity field is computed, the velocities at the positions of any vortex

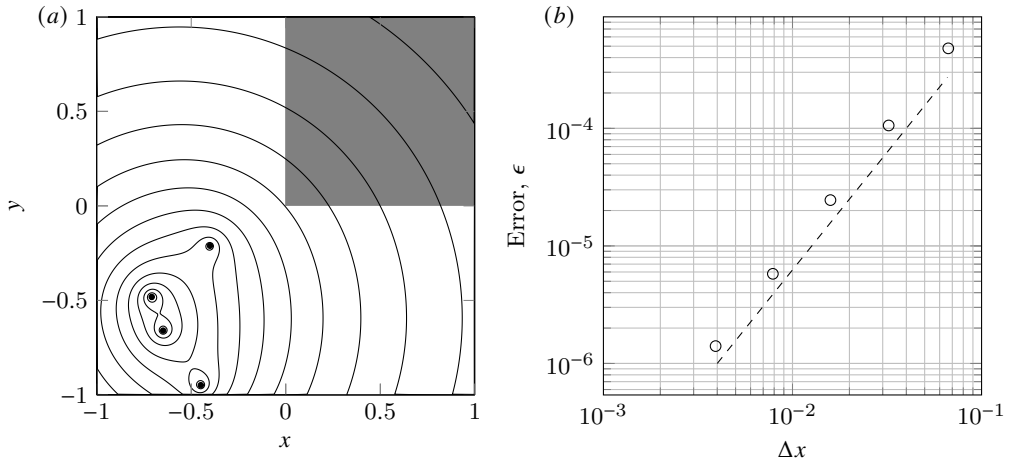


FIGURE 1. (a) Contours of the discrete streamfunction for randomly positioned point vortices (●) of random strengths, and (b) its error (○) over the shaded area for different grid spacings. Overlaid is an error (---) that scales as  $\Delta x^2$ .

element in the domain can be computed through interpolation,

$$(U_q, V_q) = \sum_{i,j} v_{ij}^N d \left( \frac{x_i - X_q}{\Delta x} \right) \left( \frac{y_j - Y_q}{\Delta x} \right), \quad (2.4)$$

where  $v^N$  is  $v$  interpolated to the nodes to obtain an overall interpolation scheme that is consistent with (2.2).

The grid differencing operators  $L$  and  $C$ , and others not yet defined, only comprise differences between grid values and do not scale their results by the grid spacing. Thus, the discrete fields require re-scaling by this grid spacing to form approximations to their continuous analogs. By convention, we assume  $v$  to serve directly as an approximation for the continuous velocity field. Thus,  $s$  is approximately equal to the continuous streamfunction divided by  $\Delta x$ , and  $w$  is approximately the continuous vorticity *multiplied by*  $\Delta x$ .

The particular solution of equation (2.1) can be written down immediately with the help of the lattice Green's function for  $L$  (Katsura & Inawashiro 1971; Cserti 2000; Liska & Colonius 2014). We denote this simply by the inverse operator,

$$\mathbf{s} = -L^{-1}\mathbf{w}. \quad (2.5)$$

It can be shown that, with a suitable truncation of the grid, both  $L$  and its inverse are symmetric operators. However,  $L$  is only positive semi-definite, and an additional homogeneous solution,  $\mathbf{s}_\infty \in \mathcal{N}$ —for example, corresponding to a uniform flow—can be added to the particular solution of this equation  $-L^{-1}\mathbf{w} + \mathbf{s}_\infty$ . This homogeneous solution allows us to satisfy boundary conditions at (discrete) infinity. The size of the domain in our simulations is therefore not relevant, as long as it includes the features that are of interest.

Figure 1 shows a mesh refinement analysis for a flow consisting of point vortices of random strength that are randomly positioned in the lower-left quadrant of the domain. The analysis verifies that the discretization technique of the Poisson equation is second-order accurate in  $\Delta x$ . We compute the error as  $\epsilon = \|\psi(x, y)/\Delta x - \mathbf{s}\|_2 / \|\mathbf{s}\|_2$ , where  $\psi$  is the exact solution for the streamfunction. We only consider the values in the upper right quadrant of the domain to exclude the positions of the point vortices, because the exact singularities at these positions are not comparable to the regularized, discrete version.

## 2.2. Potential flow with an impenetrable surface

Now, let us suppose we have a rigid impenetrable surface, on which we seek to enforce the no-penetration condition.

### 2.2.1. Discrete surface and its immersion in the grid

We carry this out at a finite number  $N$  of discrete surface forcing points; the space of scalar data on these points is denoted by  $\mathcal{S}^N$ . In particular, let us define  $r_x, r_y \in \mathcal{S}^N$  as the vectors of  $x$  and  $y$  coordinates of the surface points. Each surface point  $p$  is associated with a small straight segment of length  $\delta S_p$ . Some of the calculations will require information about the local surface orientation. For this purpose, we define vectors  $n_x, n_y \in \mathcal{S}^N$  of components of the discrete surface normals multiplied by the length of the surface segment  $\delta S_p$ . For convenience, let us also define unit vectors  $e_p$  on this space, equal to 1 at surface point  $p$  ( $1 \leq p \leq N$ ) and zero at every other point. For example, the  $x$  coordinate of point  $p$  is picked out of the vector  $r_x$  by projection onto the  $p$ th unit vector:

$$e_p^T r_x. \quad (2.6)$$

Another vector we will make substantial use of in this paper is  $\mathbf{1} \in \mathcal{S}^N$ , a vector of ones on all surface points.

From any vector  $v \in \mathcal{S}^N$ , we can also form a diagonal  $N \times N$  operator  $D_v$  with the entries of the vector along the diagonal. When this operator acts upon another vector  $w \in \mathcal{S}^N$ , it represents the Hadamard (i.e., element-by-element) product of the two vectors,  $D_v w = v \circ w \in \mathcal{S}^N$ . Note that  $D_v w = D_w v$ , and that  $D_v \mathbf{1} = v$ .

Surface data are immersed into the grid with the *regularization operator*  $R : \mathcal{S}^N \mapsto \mathcal{N}$ .  $R$  represents the same operation as applying (2.2) repeatedly to transfer  $\Gamma_{v,k}/\Delta x$  from all vortex elements to the nodes, but operates on arbitrary surface data instead. Grid data are interpolated onto the surface points with the *interpolation operator*  $E : \mathcal{N} \mapsto \mathcal{S}^N$ .  $E$  represents the same operation as applying (2.4) repeatedly for all grid points but transfers grid data to surface points instead of vortex elements. It should be noted that  $E$  can be constructed (and we will assume it has) so that it is the transpose of the interpolation operator,  $E = R^T$ .

### 2.2.2. The immersed surface potential flow problem

The surface's motion is specified by a velocity distribution  $v_b$ , represented discretely by components  $v_{b,x}, v_{b,y} \in \mathcal{S}^N$ . The no-penetration condition asserts that the normal components of the fluid velocity and this surface velocity must be equal. For rigid bodies, this surface motion can be alternatively described by a streamfunction, and the no-penetration condition can be imposed equivalently (in two dimensions) by setting the fluid streamfunction equal to that of the surface  $s_b \in \mathcal{S}^N$ , up to a uniform value,  $s_0 \in \mathcal{S}^N$ . Specifically, translation at velocity  $(U, V)$  and rotation at angular velocity  $\Omega$  would be described equivalently by velocity components

$$v_{b,x} = U\mathbf{1} - \Omega r_y, \quad v_{b,y} = V\mathbf{1} + \Omega r_x \quad (2.7)$$

or by a surface streamfunction

$$s_b = U r_y - V r_x - \frac{1}{2} \Omega \left( D_{r_x} r_x + D_{r_y} r_y \right). \quad (2.8)$$

Thus, the discrete no-penetration constraint on streamfunction is

$$E s = s_b - E s_\infty - s_0. \quad (2.9)$$

For later shorthand, we will denote the difference between the body motion streamfunction and interpolated uniform flow streamfunction by  $s'_b \equiv s_b - E s_\infty$ . This modified streamfunction simply consists of subtracting the components  $(U_\infty, V_\infty)$  of the uniform flow from  $(U, V)$  in (2.8). The

uniform value  $s_0$  is left unspecified and will later serve the role of enforcing a constraint on circulation. For now, we will suppose that it can be set arbitrarily.

The no-penetration constraint is enforced in the basic potential flow problem (2.1) with the help of a vector of Lagrange multipliers,  $f \in \mathcal{S}^N$ , on the surface points. The modified potential flow problem is thus

$$Ls + Rf = -w. \quad (2.10)$$

In fact, by simple comparison with the vorticity on the right-hand side, it is clear that the vector  $f$  represents the strength of the discrete bound vortex sheet on the surface. Suppose we consider the bound vortex sheet  $\gamma(s)$  that emerges from the analogous continuous problem on the undiscretized surface, where  $s$  is the arc-length parameter along the surface. At each point  $p$ , the discrete solution  $f$  is approximately equal to this continuous solution, multiplied by the length  $\delta S_p$  of the small segment surrounding the point:

$$e_p^T f \approx \gamma(s_p) \delta S_p. \quad (2.11)$$

Thus, the potential flow problem in the presence of the impenetrable surface is

$$\begin{bmatrix} L & R \\ E & 0 \end{bmatrix} \begin{pmatrix} s \\ f \end{pmatrix} = \begin{pmatrix} -w \\ s'_b - s_0 \end{pmatrix}. \quad (2.12)$$

This problem (2.12) has the structure of a generic *saddle-point problem* (Benzi *et al.* 2005). We will encounter many such systems in this work, so in appendix A we summarize a solution approach, based on block-LU decomposition. The generated solution algorithm of (2.12) is

$$Ls^* = -w \quad (2.13)$$

$$Sf = s'_b - s_0 - Es^* \quad (2.14)$$

$$s = s^* - L^{-1}Rf, \quad (2.15)$$

where the Schur complement  $S$  is

$$S = -EL^{-1}R. \quad (2.16)$$

Based on the properties of the matrices comprising  $S$ , this operator is symmetric and negative definite, and therefore invertible. Its inverse  $S^{-1}$ , also symmetric, maps a surface distribution of streamfunction to a corresponding bound vortex sheet strength.

We can describe this algorithm in words: First, solve for the intermediate streamfunction field, associated with vorticity in the fluid, but without regard for the presence of the surface. Second, find the bound vortex sheet whose associated streamfunction cancels the difference between the specified streamfunction on the surface and the intermediate streamfunction evaluated on the surface. Finally, correct the intermediate streamfunction field for the influence of the bound vortex sheet. A version of the Julia code that implements this algorithm, as well as the algorithms in the following sections, is available at the Github repository [Beckers & Eldredge \(2021\)](#).

We give two examples of the streamfunction with a body present and show the associated vortex sheet strength. Figure 2 shows a vortex near a circular cylinder and figure 3 shows a circular cylinder that translates horizontally. In both cases, the vortex sheet strength is in very good agreement with the exact solution from potential flow theory.

For later use, we note that the solution of (2.12) can also be written in inverse form using equation (A 7):

$$\begin{pmatrix} s \\ f \end{pmatrix} = \begin{bmatrix} L^{-1} + L^{-1}RS^{-1}EL^{-1} & -L^{-1}RS^{-1} \\ -S^{-1}EL^{-1} & S^{-1} \end{bmatrix} \begin{pmatrix} -w \\ s'_b - s_0 \end{pmatrix}. \quad (2.17)$$

The matrix operator in (2.17) is the inverse of the basic saddle-point system.

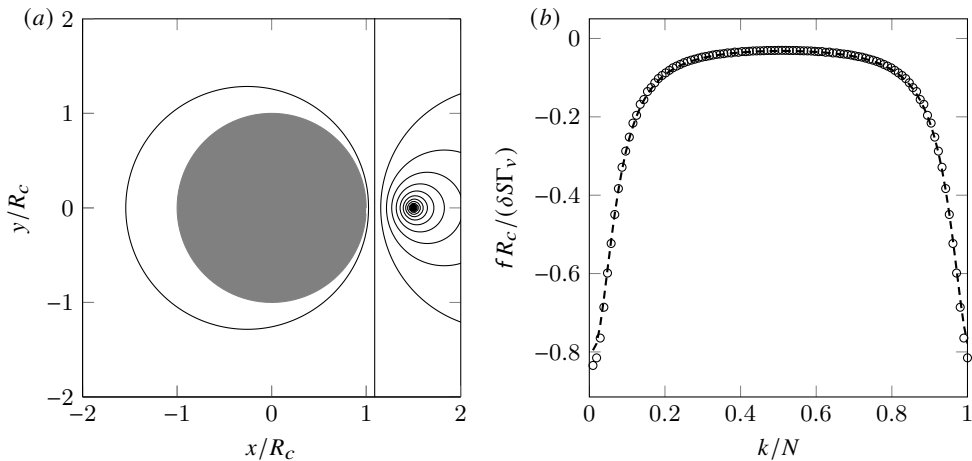


FIGURE 2. (a) Contours of the discrete streamfunction for a point vortex ( $\bullet$ ) with strength  $\Gamma_v$  at  $(R_v, 0)$  near a circular cylinder consisting of  $N$  points with radius  $R_c$  and  $R_v/R_c = 3/2$ , and (b) its scaled discrete vortex sheet strength ( $\circ$ ) in function of the normalized surface point index  $k/N$ .  $k = 1$  corresponds to the right-most point on the surface. Overlaid is the exact continuous solution (---). The simulation is performed with  $\Delta x/R_c = 0.03$  and  $\delta S/\Delta x = 2$ .

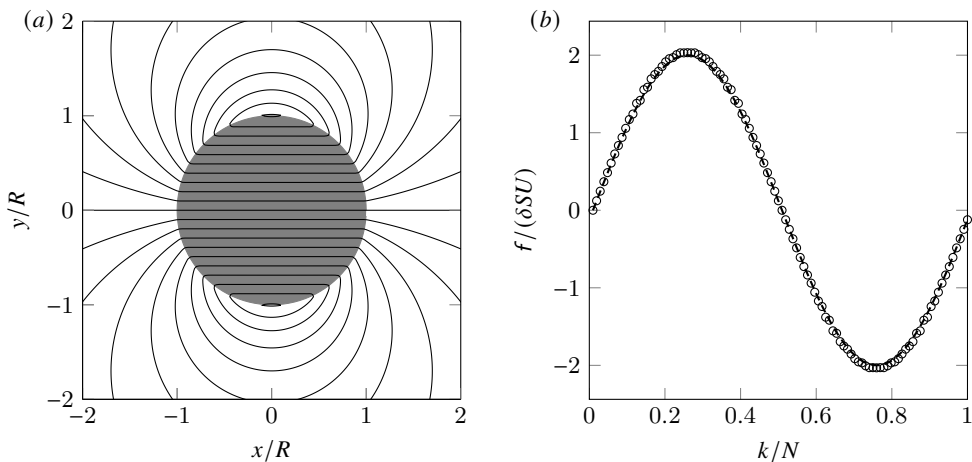


FIGURE 3. (a) Contours of the discrete streamfunction for a horizontally translating circular cylinder with radius  $R$ , and (b) its scaled discrete vortex sheet strength ( $\circ$ ). Overlaid is the exact continuous solution (---). The simulation is performed with  $\Delta x/R = 0.03$  and  $\delta S/\Delta x = 2$ .

### 2.3. Non-uniqueness and discrete circulation

In two-dimensional potential flows, there is no unique solution to problem (2.12), since one can choose any value for the uniform value  $s_0$  and still enforce the no-penetration condition. Equivalently, we can specify any *circulation* about the body and still enforce this condition. Let us determine the relationship between  $s_0$  and circulation. For later use, let us write this uniform surface streamfunction as  $s_0 = s_0 \mathbf{1}$ , where  $s_0$  is a single scalar value. The *discrete circulation*  $\Gamma_b$  about the body is given by the sum of the bound vortex sheet data and can be written compactly as

$$\Gamma_b = \mathbf{1}^T f. \quad (2.18)$$

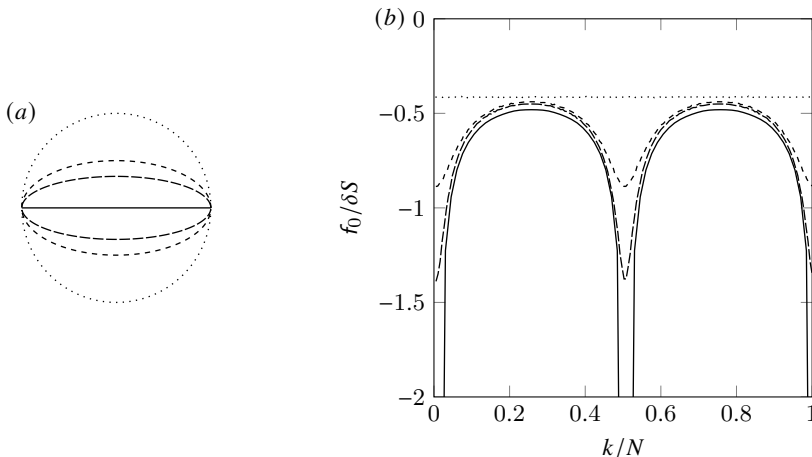


FIGURE 4. (a) Geometry and (b) the scaled bound vortex sheet strength associated with a uniform, unit-strength streamfunction for elliptical cylinders with different aspect ratios ( $AR$ ):  $\cdots$ ,  $AR = 1$ ;  $---$ ,  $AR = 2$ ;  $-.-$ ,  $AR = 3$ ;  $---$ ,  $AR = \infty$  (flat plate). The simulations are performed with  $\Delta x/R = 0.004$  and  $\delta S/\Delta x = 3$ .

The circulation of the vortex sheet in the solution (2.14) is

$$\Gamma_b = \mathbf{1}^T \mathbf{S}^{-1} \left( \mathbf{s}'_b + \mathbf{E} \mathbf{L}^{-1} \mathbf{w} \right) - s_0 \mathbf{1}^T \mathbf{S}^{-1} \mathbf{1}. \quad (2.19)$$

The scalar factor  $\mathbf{1}^T \mathbf{S}^{-1} \mathbf{1}$  in this expression is a property of the set of points and their immersion into the Cartesian grid. Part of this factor,  $\mathbf{S}^{-1} \mathbf{1}$ , represents the bound vortex sheet strength associated with a uniform, unit-strength streamfunction on the surface. This sheet has a particularly important role in some of the discussion to follow, so we will denote its strength by  $f_0$ :

$$f_0 \equiv \mathbf{S}^{-1} \mathbf{1}. \quad (2.20)$$

The transpose of  $f_0$ , equal to  $\mathbf{1}^T \mathbf{S}^{-1}$ , calculates the circulation of the associated bound vortex sheet when it acts upon a surface streamfunction. Thus, the factor  $\mathbf{1}^T \mathbf{S}^{-1} \mathbf{1}$  is the circulation associated with a uniform, unit-strength surface streamfunction. We will refer to this as  $\Gamma_0$ :

$$\Gamma_0 \equiv \mathbf{1}^T \mathbf{S}^{-1} \mathbf{1} \equiv f_0^T \mathbf{1} \equiv \mathbf{1}^T f_0. \quad (2.21)$$

Figure 4 demonstrates the distribution of  $f_0$  for elliptical cylinders with different aspect ratios. For a circular cylinder,  $f_0$  assumes a uniform distribution, which agrees with the fact that tangential velocity around a circular cylinder with non-zero circulation is constant at a given radius. When the aspect ratio increases, the distribution gradually shows stronger variations near the edges of the major axis and eventually turns singular for the flat plate. This will be discussed in more detail in the next section.

The last term in (2.19) illustrates the direct relationship between the scalar value  $s_0$  and the bound circulation  $\Gamma_b$ , and one can interpret  $s_0$  as a means of setting the circulation. Thus far, the value  $s_0$  has not been fixed. We will use it in the next section to enforce the Kutta condition. However, we will use it here for an immediate purpose. The prescribed surface streamfunction  $s'_b$  (given by (2.8), with the uniform flow accounted for) may have some associated bound circulation, and it is desirable to adjust it by adding or subtracting a uniform value so that it has none. Equation (2.19) suggests that this circulation can be removed by setting  $s_0$  to  $\mathbf{1}^T \mathbf{S}^{-1} \mathbf{s}'_b / \Gamma_0$  and then subtracting this value (multiplied by the uniform vector  $\mathbf{1}$ ) from  $s'_b$ . Overall, this process



can be encapsulated in a *circulation removal* operator that acts upon the surface streamfunction

$$\mathbf{P}^\Gamma \equiv \mathbf{I} - \frac{\mathbf{1}\mathbf{1}^T}{\Gamma_0} \mathbf{S}^{-1}. \quad (2.22)$$

It is easy to verify that  $\mathbf{1}^T \mathbf{S}^{-1} \mathbf{P}^\Gamma = 0$ , so that the circulation of any surface streamfunction acted upon by  $\mathbf{P}^\Gamma$  is indeed zero. It is important to observe, also, that  $\mathbf{s}'_b$  can be replaced by  $\mathbf{P}^\Gamma \mathbf{s}'_b$  without affecting the nature of the no-penetration condition. We also note that the composite operator  $\mathbf{S}^{-1} \mathbf{P}^\Gamma$  is symmetric, just as  $\mathbf{S}^{-1}$  is:

$$\mathbf{S}^{-1} \mathbf{P}^\Gamma = \mathbf{S}^{-1} - \frac{\mathbf{S}^{-1} \mathbf{1}\mathbf{1}^T \mathbf{S}^{-1}}{\Gamma_0} = \mathbf{S}^{-1} - \frac{\mathbf{f}_0 \mathbf{f}_0^T}{\Gamma_0}. \quad (2.23)$$

#### 2.4. The Kutta condition

For surfaces that contain convex edges, the vortex sheet strength assumes a singular behavior in the vicinity of these edges, with a strength that depends on the interior angle of the edge: sharper edges have more singular behavior. In the discrete representation of the surface, edges are only approximately represented by the sudden disruptions of positions in clusters of adjacent points. The behavior in this discrete form is not quite singular, but the solution of (2.14) nonetheless exhibits a large and rapid change of amplitude.

If we seek to eliminate this behavior, we must first have some means of exposing it. In fact, for any discretized surface, the essence of this nearly-singular behavior lies in the vector  $\mathbf{f}_0$ , and all other bound vortex sheets associated with the same surface share the same nearly-singular behavior. Thus, we will use a multiplicative decomposition of the vortex sheet strength:

$$\mathbf{f} = \mathbf{f}_0 \circ \tilde{\mathbf{f}}, \quad (2.24)$$

where  $\circ$  is the Hadamard product. This decomposed form isolates the singular behavior into  $\mathbf{f}_0$ , and  $\tilde{\mathbf{f}}$  is a relatively smoother vector of surface point data. In the regularization operation on  $\mathbf{f}$ , we can absorb  $\mathbf{f}_0$  into  $\mathbf{R}$ , first noting that the Hadamard product can alternatively be written with the help of a diagonal matrix,

$$\mathbf{f} = \mathbf{f}_0 \circ \tilde{\mathbf{f}} = \mathbf{D}_{\mathbf{f}_0} \tilde{\mathbf{f}}. \quad (2.25)$$

Then, we can define a re-scaled regularization operator,

$$\mathbf{R}\mathbf{f} = \mathbf{R}\mathbf{D}_{\mathbf{f}_0} \tilde{\mathbf{f}} = \tilde{\mathbf{R}} \tilde{\mathbf{f}}. \quad (2.26)$$

The re-scaled operator  $\tilde{\mathbf{R}} = \mathbf{R}\mathbf{D}_{\mathbf{f}_0}$  can, in turn, be absorbed into the Schur complement, defining  $\tilde{\mathbf{S}} = -\mathbf{E}\mathbf{L}^{-1} \tilde{\mathbf{R}} = \mathbf{S}\mathbf{D}_{\mathbf{f}_0}$ . A useful property of  $\tilde{\mathbf{S}}$  is that it preserves uniform vectors:

$$\tilde{\mathbf{S}}\mathbf{1} = \mathbf{S}\mathbf{D}_{\mathbf{f}_0}\mathbf{1} = \mathbf{S}\mathbf{f}_0 = \mathbf{1}, \quad \tilde{\mathbf{S}}^{-1}\mathbf{1} = \mathbf{1}. \quad (2.27)$$

The decomposition of the vortex sheet strength is demonstrated in figure 5 for a flat plate in a uniform flow. The original vortex sheet strength shows large amplitude variations at the leading and trailing edge, corresponding to large variations in the flow velocity field as the flow tries to make its way around the edges. By use of decomposition (2.24), these discrete singularities are retained in  $\mathbf{f}_0$  and we are left with a smooth  $\tilde{\mathbf{f}}$ , which varies linearly from the leading edge ( $k = 1$ ) to the trailing edge ( $k = N$ ).

The Kutta condition corresponds to annihilating the nearly-singular behavior at a surface point. At such points, we will set the corresponding value of  $\tilde{\mathbf{f}}$  to zero. Suppose we wish to enforce the Kutta condition at an edge corresponding to surface point  $k$ . The condition is

$$\mathbf{e}_k^T \tilde{\mathbf{f}} = 0. \quad (2.28)$$

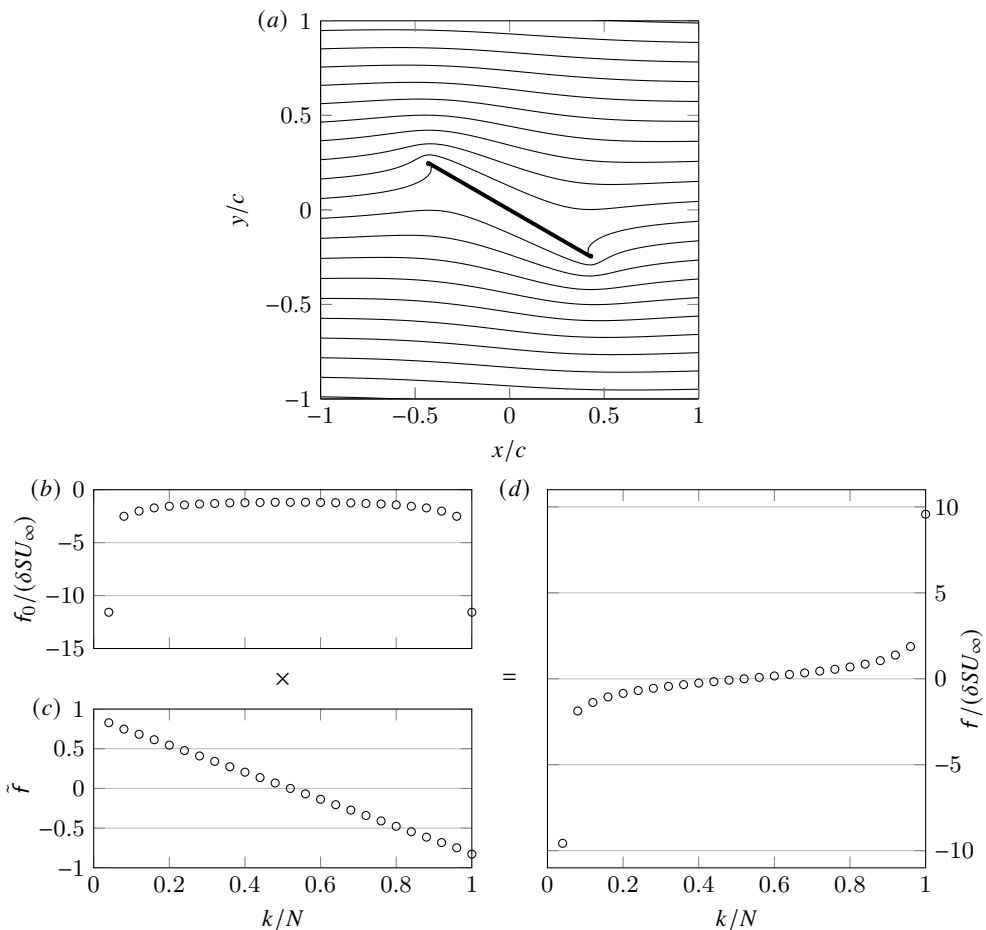


FIGURE 5. (a) Contours of the discrete streamfunction for a flat plate of length  $c$  at  $30^\circ$  in a uniform flow  $U_\infty$  without enforcement of the Kutta condition. The point-wise product of (b) the discrete vortex sheet strength associated with a uniform, unit-strength streamfunction on the body, and (c) the smooth vector that results from re-scaling the regularization operator, composes (d) the discrete vortex sheet strength. The simulation is performed with  $\Delta x/c = 0.01$  and  $\delta S/\Delta x = 4$ .

#### 2.4.1. Using the Kutta condition in a steady-state problem

We will first take the steady-state approach to enforce the Kutta condition: allow the bound circulation to be set appropriately, with the implicit understanding that there is a starting vortex of equal and opposite circulation at infinity that preserves the Kelvin circulation theorem. The Lagrange multiplier for this constraint will not be  $\Gamma_b$ , but  $s_0$ . We also use the circulation removal operator to adjust the imposed surface streamfunction:

$$\begin{bmatrix} \mathbf{L} & \tilde{\mathbf{R}} & \mathbf{0} \\ \mathbf{E} & \mathbf{0} & \mathbf{1} \\ \mathbf{0} & \mathbf{e}_k^T & \mathbf{0} \end{bmatrix} \begin{pmatrix} \mathbf{s} \\ \tilde{f} \\ s_0 \end{pmatrix} = \begin{pmatrix} -\mathbf{w} \\ \mathbf{P}^\Gamma \mathbf{s}'_b \\ \mathbf{0} \end{pmatrix} \quad (2.29)$$

This block system, like the earlier one in (2.12), has a saddle point form, and we can reduce it by the same block-LU decomposition to develop a solution algorithm. We will interpret it in the general form (A.3), with the upper left  $2 \times 2$  block taking the role of  $\mathcal{A}$ , the solution vector  $\mathbf{x}$  and

constraint force  $\mathbf{y}$  set, respectively, to

$$\mathbf{x} = \begin{pmatrix} \mathbf{s} \\ \tilde{f} \end{pmatrix}, \quad \mathbf{y} = s_0, \quad (2.30)$$

the remaining operators set to

$$\mathcal{B}_2 = [0 \quad e_k^T], \quad \mathcal{B}_1^T = \begin{bmatrix} 0 \\ 1 \end{bmatrix}, \quad C = 0, \quad (2.31)$$

and the right-hand side vectors set to

$$\mathbf{r}_1 = \begin{pmatrix} -\mathbf{w} \\ \mathbf{P}^\Gamma s'_b \end{pmatrix}, \quad \mathbf{r}_2 = 0. \quad (2.32)$$

We note that block  $\mathcal{A}$  has the original form of the system before the Kutta constraint (2.12), though with the slight modification of a re-scaled regularization operator, and we already have the inverse of  $\mathcal{A}$  available from (2.17). The solution of this original system forms the intermediate solution of the full system endowed with the Kutta condition:

$$\tilde{f}^* = \tilde{\mathcal{S}}^{-1} \left( \mathbf{P}^\Gamma s'_b + \mathbf{E}\mathbf{L}^{-1}\mathbf{w} \right), \quad \mathbf{s}^* = -\mathbf{L}^{-1} \left( \mathbf{w} + \tilde{\mathbf{R}}\tilde{f}^* \right). \quad (2.33)$$

Then, using the general procedure outlined in appendix A, the solution of the full system (2.29) is easy to develop; its Schur complement is simply

$$\mathcal{S} = -1. \quad (2.34)$$

Applying the general solution equations, and using the property (2.27) to simplify the resulting operators, it can be shown that the solution is

$$s_0 = e_k^T \tilde{f}^* \quad (2.35)$$

$$\begin{pmatrix} \mathbf{s} \\ \tilde{f} \end{pmatrix} = \begin{pmatrix} \mathbf{s}^* \\ \tilde{f}^* \end{pmatrix} - \begin{bmatrix} -\mathbf{L}^{-1}\tilde{\mathbf{R}}\mathbf{1} \\ 1 \end{bmatrix} e_k^T \tilde{f}^*. \quad (2.36)$$

The entire solution can be written more compactly as

$$\tilde{f} = \mathbf{P}_k^K \tilde{\mathcal{S}}^{-1} \left( \mathbf{P}^\Gamma s'_b + \mathbf{E}\mathbf{L}^{-1}\mathbf{w} \right), \quad (2.37)$$

$$\mathbf{s} = -\mathbf{L}^{-1} \left( \mathbf{w} + \tilde{\mathbf{R}}\tilde{f} \right), \quad (2.38)$$

where we have defined the *Kutta projection operator*,

$$\mathbf{P}_k^K \equiv \mathbf{I} - \mathbf{1}e_k^T, \quad (2.39)$$

which acts upon the (smooth part of the) bound vortex sheet vector, subtracting the value at point  $k$  from every point, including at  $k$  itself.

The application of the Kutta condition to a steady-state problem is demonstrated in Figure 6 on the flat plate problem that was introduced in the previous section. By constraining the trailing edge point of  $\tilde{f}$ , its whole distribution is shifted upward such that the last value equals zero. The resulting streamfunction indicates that the flow then indeed smoothly leaves the trailing edge.

Note that the Lagrange multiplier for the Kutta condition takes the simple value given by equation (2.35), revealing that the additional streamfunction on the surface is exactly the value of the intermediate bound vortex sheet at the Kutta point  $k$ .

#### 2.4.2. Using the Kutta condition to set a new vortex element

In the previous section, we used the Kutta condition to set the bound circulation but did not explicitly create a new vortex element. This vortex element was assumed to lie at infinity so that its effect was negligible except insofar as it left equal but opposite circulation about the body.

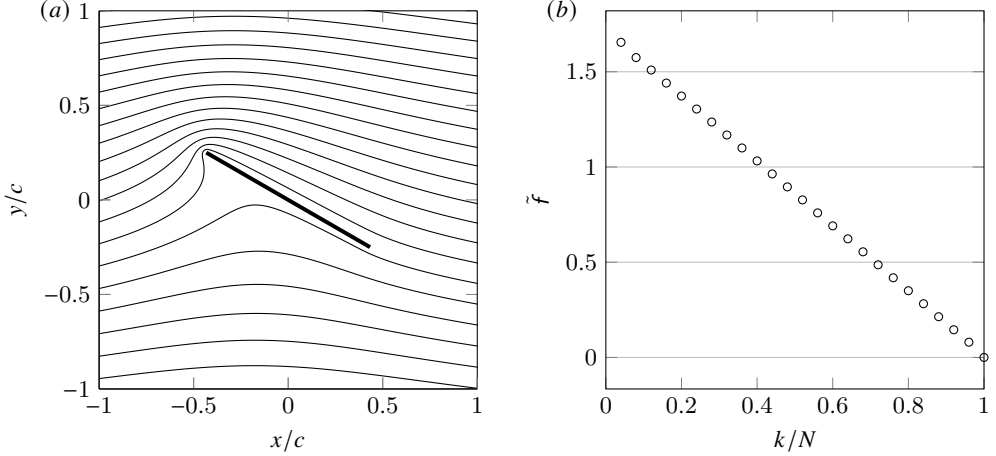


FIGURE 6. (a) Contours of the steady, discrete streamfunction for a flat plate of length  $c$  at  $30^\circ$  in a uniform flow with enforcement of the Kutta condition at the trailing edge, and (b) the smooth part of the associated discrete vortex sheet strength. The simulation is performed with  $\Delta x/c = 0.01$  and  $\delta S/\Delta x = 4$ .

In this section, we will create a new vortex element in the vicinity of the edge at which we are applying the Kutta condition. We will thus seek to establish the strength of this new element and to do so in such a manner that the overall circulation of the flow is conserved. Once the element is created, it will be allowed to advect with the local fluid velocity (minus its own contribution to this velocity).

Let us assume that the new vortex element (which we label with the subscript 1) is introduced at some point in physical space, and that its immersion into the Cartesian grid is described by a grid vector  $\mathbf{d}_1 \in \mathcal{N}$  and that its strength (i.e., its circulation) is  $\delta\Gamma_1$ . Thus, the fluid vorticity after this new element's introduction can be written as

$$\mathbf{w} + \delta\Gamma_1 \mathbf{d}_1. \quad (2.40)$$

The vector  $\mathbf{d}_1$  is the discrete Dirac delta function, identical (or similar) to the function that constitutes the regularization  $\mathbf{R}$  and interpolation  $\mathbf{E}$  matrices.

Kutta condition (2.28) is still to be enforced. We also seek to ensure that the total circulation is zero. (We are assuming that the flow has started from rest.) Let us denote the circulation of the existing fluid vorticity  $\mathbf{w}$  by

$$\Gamma_w = \Delta x \mathbf{1}^T \mathbf{w}, \quad (2.41)$$

where  $\mathbf{1} \in \mathcal{N}$  is a grid vector of ones. Then, the circulation constraint is

$$\mathbf{1}^T \mathbf{f} + \delta\Gamma_1 + \Gamma_w = 0. \quad (2.42)$$

The circulation of the bound vortex sheet  $\mathbf{f}$  can be re-written in terms of the smooth part of the sheet as  $\mathbf{1}^T \mathbf{f} = \mathbf{f}_0^T \tilde{\mathbf{f}}$ .

With these two constraints, the overall saddle point system of equations is

$$\begin{bmatrix} \mathbf{L} & \tilde{\mathbf{R}} & \mathbf{0} & \mathbf{d}_1 \\ \mathbf{E} & \mathbf{0} & \mathbf{1} & \mathbf{0} \\ \mathbf{0} & \mathbf{e}_k^T & \mathbf{0} & \mathbf{0} \\ \mathbf{0} & \mathbf{f}_0^T & \mathbf{0} & \mathbf{1} \end{bmatrix} \begin{pmatrix} \mathbf{s} \\ \tilde{\mathbf{f}} \\ s_0 \\ \delta\Gamma_1 \end{pmatrix} = \begin{pmatrix} -\mathbf{w} \\ \mathbf{P}^\Gamma \mathbf{s}'_b \\ \mathbf{0} \\ -\Gamma_w \end{pmatrix}. \quad (2.43)$$

Again, the basic saddle-point matrix constitutes the upper left  $2 \times 2$  block  $\mathcal{A}$  and the solution

vector  $\mathbf{x}$  is as before. The constraint force vector is

$$\mathbf{y} = \begin{pmatrix} s_0 \\ \delta\Gamma_1 \end{pmatrix}, \quad (2.44)$$

and the remaining vectors and operators are now

$$\mathbf{r}_2 = \begin{pmatrix} 0 \\ -\Gamma_w \end{pmatrix}, \quad \mathcal{B}_2 = \begin{bmatrix} 0 & \mathbf{e}_k^T \\ 0 & \mathbf{f}_0^T \end{bmatrix}, \quad \mathcal{B}_1^T = \begin{bmatrix} 0 & \mathbf{d}_1 \\ 1 & 0 \end{bmatrix}, \quad \mathcal{C} = - \begin{bmatrix} 0 & 0 \\ 0 & 1 \end{bmatrix}. \quad (2.45)$$

The solution algorithm follows, once again, from the equations in appendix A. After carrying out the block matrix multiplications, it can be shown that the Schur complement (A 2) is the  $2 \times 2$  matrix

$$\mathcal{S} = \begin{bmatrix} -1 & \mathbf{e}_k^T \tilde{\mathbf{f}}_1 \\ -\mathbf{f}_0^T \mathbf{1} & 1 + \mathbf{f}_0^T \tilde{\mathbf{f}}_1 \end{bmatrix} \quad (2.46)$$

where, for convenience, we have defined

$$\tilde{\mathbf{f}}_1 = \tilde{\mathbf{S}}^{-1} \mathbf{E} \mathbf{L}^{-1} \mathbf{d}_1, \quad (2.47)$$

which represents the (smooth part of the) strength of the vortex sheet that “reacts” to the presence of a unit-strength vortex  $\mathbf{d}_1$  immersed into the grid, canceling that vortex’s induced velocity on the surface. The term  $\mathbf{f}_0^T \tilde{\mathbf{f}}_1$  represents this sheet’s bound circulation and  $\mathbf{e}_k^T \tilde{\mathbf{f}}_1$  is its contribution to the Kutta condition at point  $k$ . The problem (A 6) for the constraint forces  $s_0$  and  $\delta\Gamma_1$  is then

$$\begin{bmatrix} -1 & \mathbf{e}_k^T \tilde{\mathbf{f}}_1 \\ -\mathbf{f}_0^T \mathbf{1} & 1 + \mathbf{f}_0^T \tilde{\mathbf{f}}_1 \end{bmatrix} \begin{pmatrix} s_0 \\ \delta\Gamma_1 \end{pmatrix} = \begin{pmatrix} -\mathbf{e}_k^T \tilde{\mathbf{f}}^* \\ -\Gamma_w - \mathbf{f}_0^T \tilde{\mathbf{f}}^* \end{pmatrix}. \quad (2.48)$$

The determinant of this Schur complement matrix is  $-1 - \mathbf{f}_0^T \mathbf{P}_k^K \tilde{\mathbf{f}}_1$ , which represents the negative of the circulation of the unit vortex and its associated vortex sheet, after the Kutta condition has been enforced on this sheet. It is straightforward then to calculate the strength of the new vortex  $\delta\Gamma_1$  and the additional uniform surface streamfunction,  $s_0$ :

$$\delta\Gamma_1 = \frac{-\Gamma_w - \mathbf{f}_0^T \mathbf{P}_k^K \tilde{\mathbf{f}}^*}{1 + \mathbf{f}_0^T \mathbf{P}_k^K \tilde{\mathbf{f}}_1}, \quad s_0 = \mathbf{e}_k^T \left( \tilde{\mathbf{f}}^* + \delta\Gamma_1 \tilde{\mathbf{f}}_1 \right). \quad (2.49)$$

where the intermediate solution  $\tilde{\mathbf{f}}^*$  is available from (2.33). From these, we can then obtain the vortex sheet strength and the fluid streamfunction,

$$\tilde{\mathbf{f}} = \mathbf{P}_k^K \left( \tilde{\mathbf{f}}^* + \delta\Gamma_1 \tilde{\mathbf{f}}_1 \right), \quad \mathbf{s} = -\mathbf{L}^{-1} \left( \mathbf{w} + \delta\Gamma_1 \mathbf{d}_1 + \tilde{\mathbf{R}} \tilde{\mathbf{f}} \right). \quad (2.50)$$

We now apply the method to the flat plate problem with a point vortex near the trailing edge to enforce the Kutta condition at that edge. We position the point vortex at a distance  $3\Delta t U_\infty$  from the edge in the direction of the free stream, perpendicular to the plate. Figure 7 shows that, because of the proximity of the point vortex to the flat plate,  $\tilde{\mathbf{f}}$  exhibits a quick variation in its value at the surface points that lie closest to the point vortex. The value at the trailing edge point itself is still constrained to zero and the flow again leaves the edge smoothly. This situation corresponds to the flow right after impulsively starting a uniform flow around a flat plate and the point vortex now represents the starting vortex.

### 2.4.3. Applying more than one Kutta condition on a body

Suppose we wish to enforce the Kutta condition at two edges of the body—at points  $k_1$  and  $k_2$ —instead of one. Each such point has a constraint,

$$\mathbf{e}_{k_j}^T \tilde{\mathbf{f}} = 0, \quad j = 1, 2. \quad (2.51)$$

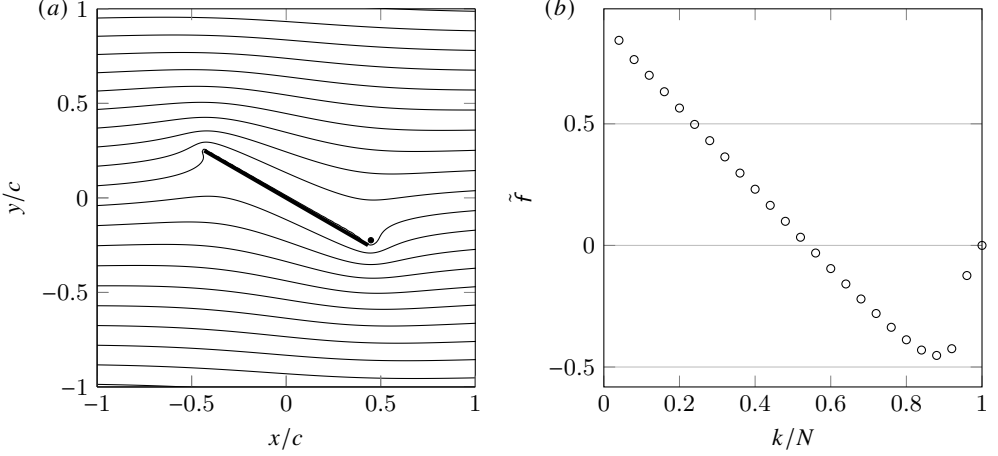


FIGURE 7. (a) Contours of the unsteady, discrete streamfunction for a flat plate of length  $c$  at  $30^\circ$  in a uniform flow with release of vorticity into a point vortex ( $\bullet$ ) for enforcement of the Kutta condition at the trailing edge. (b) The smooth part of the associated discrete vortex sheet strength. The simulation is performed with  $\Delta x/c = 0.01$  and  $\delta S/\Delta x = 4$ .

For two such constraints, we need two Lagrange multipliers: the strengths of two new vortices,  $\delta\Gamma_1$  and  $\delta\Gamma_2$ , immersed into the grid with  $\mathbf{d}_1$  and  $\mathbf{d}_2$ , respectively; and we still need the Lagrange multiplier  $s_0$  to ensure that Kelvin's circulation theorem is also enforced. The system in the previous section is thus easily generalized to the following:

$$\begin{bmatrix} \mathbf{L} & \tilde{\mathbf{R}} & 0 & \mathbf{d}_1 & \mathbf{d}_2 \\ \mathbf{E} & 0 & 1 & 0 & 0 \\ 0 & \mathbf{e}_{k_1}^T & 0 & 0 & 0 \\ 0 & \mathbf{e}_{k_2}^T & 0 & 0 & 0 \\ 0 & \mathbf{f}_0^T & 0 & 1 & 1 \end{bmatrix} \begin{pmatrix} \mathbf{s} \\ \tilde{\mathbf{f}} \\ s_0 \\ \delta\Gamma_1 \\ \delta\Gamma_2 \end{pmatrix} = \begin{pmatrix} -\mathbf{w} \\ \mathbf{P}^\Gamma \mathbf{s}'_b \\ 0 \\ 0 \\ -\Gamma_w \end{pmatrix}. \quad (2.52)$$

The system is reduced in the same manner as before, with the same intermediate solution obtained from the basic system (2.12). Now, the Schur complement problem for the constraint forces takes the form

$$\begin{bmatrix} -1 & \mathbf{e}_{k_1}^T \tilde{\mathbf{f}}_1 & \mathbf{e}_{k_1}^T \tilde{\mathbf{f}}_2 \\ -1 & \mathbf{e}_{k_2}^T \tilde{\mathbf{f}}_1 & \mathbf{e}_{k_2}^T \tilde{\mathbf{f}}_2 \\ -\mathbf{f}_0^T \mathbf{1} & 1 + \mathbf{f}_0^T \tilde{\mathbf{f}}_1 & 1 + \mathbf{f}_0^T \tilde{\mathbf{f}}_2 \end{bmatrix} \begin{pmatrix} s_0 \\ \delta\Gamma_1 \\ \delta\Gamma_2 \end{pmatrix} = \begin{pmatrix} -\mathbf{e}_{k_1}^T \tilde{\mathbf{f}}^* \\ -\mathbf{e}_{k_2}^T \tilde{\mathbf{f}}^* \\ -\Gamma_w - \mathbf{f}_0^T \tilde{\mathbf{f}}^* \end{pmatrix}, \quad (2.53)$$

where we have now defined bound vortex sheets associated with each of the two new vortices (with unit strengths):

$$\tilde{\mathbf{f}}_j = \tilde{\mathbf{S}}^{-1} \mathbf{E} \mathbf{L}^{-1} \mathbf{d}_j, \quad (2.54)$$

for  $j = 1, 2$ . It is interesting to note that, if we take the difference between the two Kutta constraints, we obtain

$$\left( \mathbf{e}_{k_1}^T - \mathbf{e}_{k_2}^T \right) \left( \tilde{\mathbf{f}}^* + \delta\Gamma_1 \tilde{\mathbf{f}}_1 + \delta\Gamma_2 \tilde{\mathbf{f}}_2 \right) = 0. \quad (2.55)$$

It can be shown that this Schur complement problem can be split into

$$\begin{bmatrix} 1 + \mathbf{f}_0^T \mathbf{P}_{k_1}^K \tilde{\mathbf{f}}_1 & 1 + \mathbf{f}_0^T \mathbf{P}_{k_1}^K \tilde{\mathbf{f}}_2 \\ 1 + \mathbf{f}_0^T \mathbf{P}_{k_2}^K \tilde{\mathbf{f}}_1 & 1 + \mathbf{f}_0^T \mathbf{P}_{k_2}^K \tilde{\mathbf{f}}_2 \end{bmatrix} \begin{pmatrix} \delta\Gamma_1 \\ \delta\Gamma_2 \end{pmatrix} = - \begin{pmatrix} \Gamma_w + \mathbf{f}_0^T \mathbf{P}_{k_1}^K \tilde{\mathbf{f}}^* \\ \Gamma_w + \mathbf{f}_0^T \mathbf{P}_{k_2}^K \tilde{\mathbf{f}}^* \end{pmatrix} \quad (2.56)$$

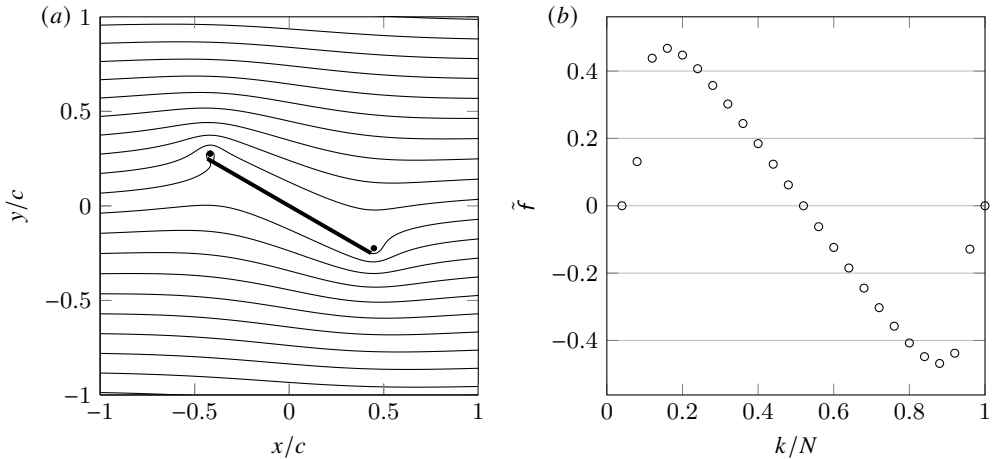


FIGURE 8. (a) Contours of the unsteady, discrete streamfunction for a flat plate of length  $c$  at  $30^\circ$  in a uniform flow with release of vorticity into two point vortices (●) for enforcement of the Kutta condition at both edges. (b) The smooth part of the associated discrete vortex sheet strength. The simulation is performed with  $\Delta x/c = 0.01$  and  $\delta S/\Delta x = 4$ .

and

$$s_0 = \frac{1}{2} \left( e_{k_1}^T + e_{k_2}^T \right) \left( \tilde{f}^* + \delta\Gamma_1 \tilde{f}_1 + \delta\Gamma_2 \tilde{f}_2 \right). \quad (2.57)$$

The latter equation, when combined with (2.55), reveals that the value of the vortex sheet strength  $\tilde{f}^* + \delta\Gamma_1 \tilde{f}_1 + \delta\Gamma_2 \tilde{f}_2$  is the same at both Kutta points and equal to  $s_0$ .

Equation (2.56) can be solved easily for the strengths of the two new point vortices. Then, the solution for the vortex sheet strength and streamfunction are

$$\tilde{f} = \frac{1}{2} \left( \mathbf{P}_{k_1}^K + \mathbf{P}_{k_2}^K \right) \left( \tilde{f}^* + \delta\Gamma_1 \tilde{f}_1 + \delta\Gamma_2 \tilde{f}_2 \right), \quad \mathbf{s} = -\mathbf{L}^{-1} \left( \mathbf{w} + \delta\Gamma_1 \mathbf{d}_1 + \delta\Gamma_2 \mathbf{d}_2 + \tilde{\mathbf{R}}\tilde{f} \right) \quad (2.58)$$

We now apply this method in figure 8 to enforce the Kutta condition at the leading and trailing edge of our flat plate problem. We position a point vortex close to each edge and observe again that  $\tilde{f}$  shows strong variation at the surface points closest to the two point vortices. The contours of the streamfunction indicate that the flow indeed leaves the edges smoothly. Like the previous case, this solution corresponds to the flow right after impulsively starting a uniform flow around a flat plate, but unlike the previous case, the flow now separates at the leading edge.

It should be observed that these solutions are posed in a manner easily extensible to an arbitrary number of edges.

### 2.5. Generalized edge condition

In the previous section, we demonstrated the means of annihilating the (nearly) singular behavior at edges on a discretized surface. In some cases, our desire is not to annihilate this behavior, but simply to keep it within some bounds. In the analytical treatment of potential flow problems, this objective is served by placing an inequality constraint on the *edge suction parameter* Ramesh *et al.* (2014); Darakananda & Eldredge (2019); Eldredge (2019). That parameter is proportional to the coefficient on the bound vortex sheet strength's singularity Eldredge (2019), so in this discrete setting, in which we have extracted the singular part of  $f$  in the form of  $f_0$ , we expect the suction parameter to be related to the value of  $\tilde{f}$  at the edge. In fact, by simple

comparison, it can be shown that

$$e_k^T \tilde{f} = -\frac{2\pi c}{\Gamma_0} \sigma_k \quad (2.59)$$

for a flat plate of length  $c$ , where  $\sigma_k$  is the suction parameter at the edge corresponding to point  $k$ .

Let  $\sigma_k^{\min}$  and  $\sigma_k^{\max}$  denote the minimum and maximum tolerable values of  $\sigma_k$  at edge  $k$ . We then seek to confine the suction parameter to the range  $\sigma_k^{\min} \leq \sigma_k \leq \sigma_k^{\max}$ . This generalized edge constraint is placed on the suction parameter of the intermediate sheet  $\tilde{f}^*$ . To avoid confusion, we will redefine the bounds based on this smooth part of the vortex sheet rather than  $\sigma_k$  itself; for this, we define  $\tilde{f}_k^{\min} = -2\pi\sigma_k^{\max}/\Gamma_0$  and  $\tilde{f}_k^{\max} = -2\pi\sigma_k^{\min}/\Gamma_0$ . Thus, we inspect whether the value  $e_k^T \tilde{f}$  lies in the range

$$\tilde{f}_k^{\min} \leq e_k^T \tilde{f}^* \leq \tilde{f}_k^{\max}. \quad (2.60)$$

If  $e_k^T \tilde{f}$  lies within this range, then no new vortex is created near the edge (or equivalently, a new vortex of zero strength is created); if  $e_k^T \tilde{f} > \tilde{f}_k^{\max}$ , then we create a new vortex so that  $e_k^T \tilde{f} = \tilde{f}_k^{\max}$ ; and if  $e_k^T \tilde{f} < \tilde{f}_k^{\min}$ , then we do the same, but now so that  $e_k^T \tilde{f} = \tilde{f}_k^{\min}$ . Note that the Kutta condition simply corresponds to setting  $\tilde{f}_k^{\min} = \tilde{f}_k^{\max} = 0$ .

We can easily accommodate these constraints into our solution approach for enforcing the Kutta condition from the previous section: in the case of two edges, by modifying the right-hand side vector of (2.56) (if the edge suction lies outside of its bounds) or setting the vortex strength corresponding to that edge to zero. For example, suppose that  $e_{k_1}^T \tilde{f}^* < \tilde{f}_{k_1}^{\min}$  and  $e_{k_2}^T \tilde{f}^* > \tilde{f}_{k_2}^{\max}$ ; then we solve the system

$$\begin{bmatrix} 1 + f_0^T \mathbf{P}_{k_1}^K \tilde{f}_1 & 1 + f_0^T \mathbf{P}_{k_1}^K \tilde{f}_2 \\ 1 + f_0^T \mathbf{P}_{k_2}^K \tilde{f}_1 & 1 + f_0^T \mathbf{P}_{k_2}^K \tilde{f}_2 \end{bmatrix} \begin{pmatrix} \delta\Gamma_1 \\ \delta\Gamma_2 \end{pmatrix} = - \begin{pmatrix} \Gamma_w + f_0^T \mathbf{P}_{k_1}^K \tilde{f}^* + \Gamma_0 \tilde{f}_{k_1}^{\min} \\ \Gamma_w + f_0^T \mathbf{P}_{k_2}^K \tilde{f}^* + \Gamma_0 \tilde{f}_{k_2}^{\max} \end{pmatrix}. \quad (2.61)$$

But if, say,  $\tilde{f}_{k_2}^{\min} \leq e_{k_2}^T \tilde{f}^* \leq \tilde{f}_{k_2}^{\max}$ , then we set  $\delta\Gamma_2 = 0$  and this system reduces to

$$\delta\Gamma_1 = -\frac{\Gamma_w + f_0^T \mathbf{P}_{k_1}^K \tilde{f}^* + \Gamma_0 \tilde{f}_{k_1}^{\min}}{1 + f_0^T \mathbf{P}_{k_1}^K \tilde{f}_1}. \quad (2.62)$$

The effect of applying these generalized edge conditions to the leading edge of a flat plate is shown in figure 9 for the first instants after impulsively starting a uniform flow. In this and the following simulations, forward Euler is used to advance the system in time. When new point vortices are inserted, they are placed one-third of the way from the edge to the last released vortex from that edge. The positions of the point vortices emanating from the leading edge in figure 9 indicate that as  $\sigma_k^{\max}$  increases, the stream of point vortices is swept back from the edge. At the trailing edge, the Kutta condition is enforced in each case and the positions of the point vortices overlap, as they are not yet influenced by the different situations at the leading edge in these first instants.

## 2.6. Force and the added mass

### 2.6.1. Impulse-based calculations of force and moment

We will develop a means of calculating the force and moment on the body through the negative rate of change of impulse in the fluid (Eldredge 2019). The continuous expressions for linear and



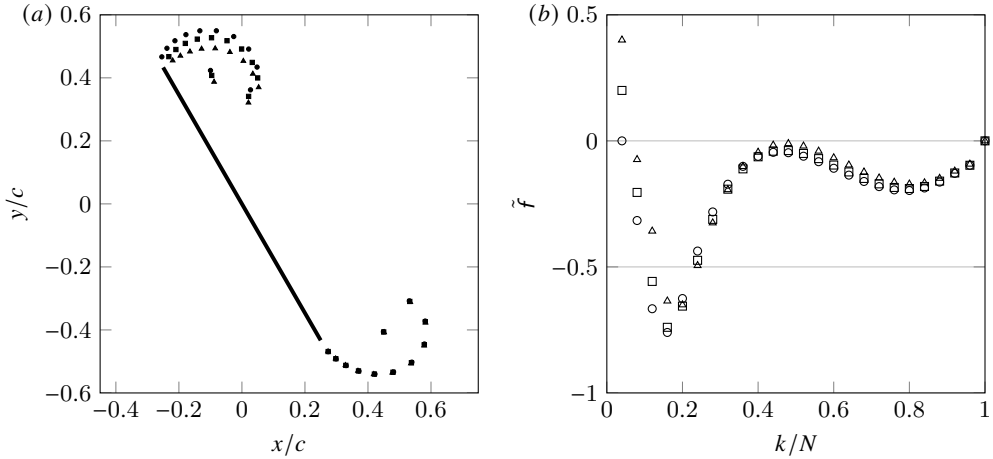


FIGURE 9. Effect of increasing  $\sigma_{LE}^{\max}/U_{\infty}$  from 0 (● and ○) to 0.15 (■ and □) and 0.3 (▲ and △) on (a) the positions of shedded point vortices and (b) the smooth part of the associated discrete vortex sheet strength for a flat plate of length  $c$  at  $60^\circ$ , 0.2 convective times after impulsively starting a uniform flow  $U_{\infty}$ . At the trailing edge, the Kutta condition is enforced. The simulation is performed with  $\Delta x/c = 0.01$ ,  $\delta S/\Delta x = 4$ , and  $\Delta t U_{\infty}/c = 0.02$ .

angular impulse (about the origin) are, in two dimensions,

$$\mathbf{P} = \int_{V_f} \mathbf{x} \times \boldsymbol{\omega} dV + \int_{S_b} \mathbf{x} \times (\mathbf{n} \times \mathbf{v}) dS \quad (2.63)$$

$$\boldsymbol{\Pi}_0 = \frac{1}{2} \int_{V_f} \mathbf{x} \times (\mathbf{x} \times \boldsymbol{\omega}) dV + \frac{1}{2} \int_{S_b} \mathbf{x} \times [\mathbf{x} \times (\mathbf{n} \times \mathbf{v})] dS \quad (2.64)$$

If there is only a single body, then the force and moment (about the origin) exerted by the fluid on that body are given by

$$\mathbf{F} = -\rho \frac{d\mathbf{P}}{dt}, \quad \mathbf{M}_0 = -\rho \frac{d\boldsymbol{\Pi}_0}{dt}, \quad (2.65)$$

where  $\rho$  is the fluid density. In the two-dimensional applications of this paper, angular impulse and the moment have only a single component, e.g.,  $\boldsymbol{\Pi}_0 = \Pi_0 \mathbf{e}_z$ , where  $\mathbf{e}_z$  is the unit vector out of the plane.

It should be observed that, by definition, the bound vortex sheet strength  $\gamma$  is equal to the jump in tangential velocity between the fluid and the surface,  $\mathbf{n} \times \mathbf{v} = \gamma \mathbf{e}_z + \mathbf{n} \times \mathbf{v}_b$ , where  $\mathbf{n}$  is the unit surface normal vector directed into the fluid,  $\mathbf{v}$  is the fluid velocity, and  $\mathbf{v}_b$  is the velocity of the surface. Thus, the surface integrals in (2.63) and (2.64) can be re-written in terms of the vortex sheet strength and the body motion.

We can easily develop discrete forms of the integrals (2.63) and (2.64) with the solutions and notation described in this paper. For the volume integrals, let us denote diagonal matrices containing the coordinates of the grid nodes by  $D_x$  and  $D_y$ . Thus, the expressions in (2.63) and (2.64) can be written in discrete form as

$$P_x = \Delta x \mathbf{y}^T \mathbf{w} + r_y^T \left( f + D_{n_x} v_{b,y} - D_{n_y} v_{b,x} \right), \quad (2.66)$$

$$P_y = -\Delta x \mathbf{x}^T \mathbf{w} - r_x^T \left( f + D_{n_x} v_{b,y} - D_{n_y} v_{b,x} \right), \quad (2.67)$$

and

$$\Pi_0 = -\frac{1}{2} \Delta x \left( \mathbf{x}^T D_x + \mathbf{y}^T D_y \right) \mathbf{w} - \frac{1}{2} \left( r_x^T D_{r_x} + r_y^T D_{r_y} \right) \left( f + D_{n_x} v_{b,y} - D_{n_y} v_{b,x} \right). \quad (2.68)$$

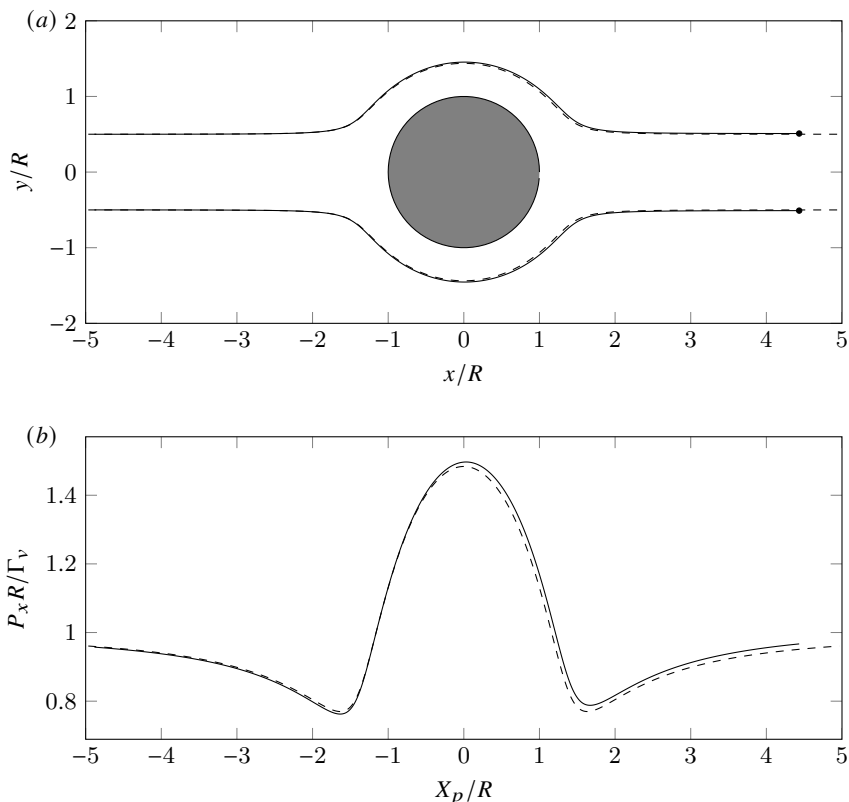


FIGURE 10. (a) Numerically simulated trajectories (—) of two point vortices (●) of opposite strengths  $\Gamma_v$  and  $-\Gamma_v$  being convected past a circular cylinder with radius  $R$ , and (b) the  $x$  component of the associated, numerically simulated impulse (—) in the fluid. Overlaid are the exact continuous trajectories (- - -) and impulse (- - -). The simulation is performed with  $\Delta x/c = 0.04$ ,  $\delta S/\Delta x = 2$ , and  $\Delta t \Gamma_v/R^2 = 0.1$ .

The overall force and moment exerted on the body are obtained from calculating these impulses and computing their rates of change in (2.65). Part of this force and moment is attributable to the dynamics of vorticity in the fluid. The remaining part is due to surface motion relative to the fluid, and we will discuss this in the next section.

To illustrate the accuracy of the impulse-based calculation of force, we apply the method to two examples. In the first example, we simulate the trajectories of two point vortices of opposite strength, convected by each other past a cylinder. Figure 10 shows the trajectories and the  $x$  component of the impulse together with their exact solutions. It is clear from the figure that the simulation shows very good agreement with the exact solution. In the second example, we compare our simulation of the first instants of the unsteady, fully separated flow around a flat plate after impulsively starting a uniform flow with the Biot-Savart method from Darakananda & Eldredge (2019), using the same positioning rules to insert point vortices and the same time step. The vortex positions and the corresponding impulse and lift are compared in figure 11 and show very good agreement as well.

### 2.6.2. Added mass

The added mass tensor provides a measure of the inertial influence of the fluid on the body in response to changes in the body's translational or rotational motion. The coefficients of the added mass tensor of a body are obtained by computing the impulse components associated with

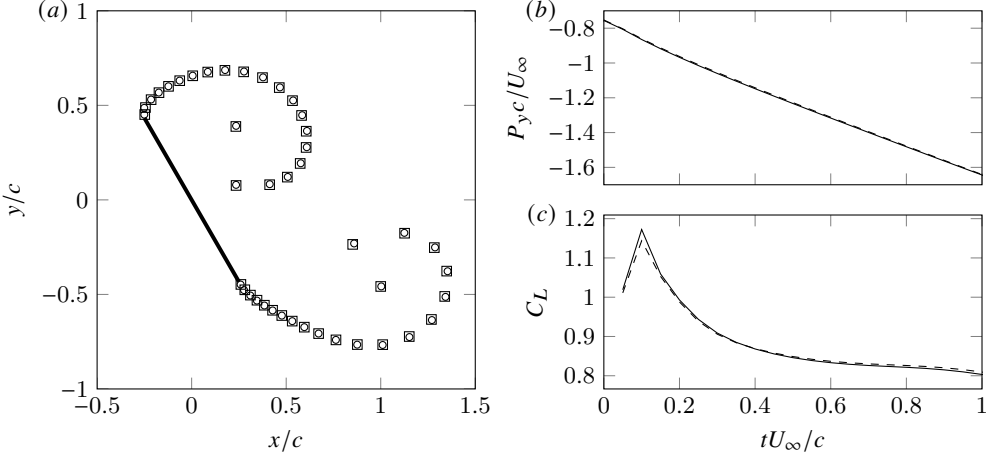


FIGURE 11. Comparison of the simulated vortex shedding behind a flat plate of length  $c$  at  $60^\circ$  in a uniform flow using the method in this paper ( $\circ$  and —) and using the Biot-Savart method of Darakananda & Eldredge (2019) ( $\square$  and - - -). (a) The positions of the shedded point vortices, (b) the vertical component of the associated impulse, and (c) the lift coefficient, one convective time after impulsively starting the uniform flow. At both edges, the Kutta condition is enforced. The simulation is performed with  $\Delta x/c = 0.01$ ,  $\delta S/\Delta x = 2$ , and  $\Delta t U_\infty/c = 0.05$ .

a unit-valued component of motion (Eldredge 2019). The motion's influence is both direct, via the surface velocity, and indirect, in the bound vortex sheet that develops on the surface.

For example, suppose that we consider translation at unit velocity in the  $x$  direction, for which the motion is described by  $v_{b,x} = 1$ ,  $v_{b,y} = 0$ , and  $s'_b = r_y$ , and the associated bound vortex sheet—obtained without Kutta condition by solving the basic problem (2.12)—is  $f = \mathbf{S}^{-1} \mathbf{P}^\Gamma s'_b = \mathbf{S}^{-1} \mathbf{P}^\Gamma r_y$ . The added mass coefficients corresponding to this motion are derived by substituting these into the impulse formulas (2.66)–(2.68):

$$P_x^{(x)} = r_y^T \left( \mathbf{S}^{-1} \mathbf{P}^\Gamma r_y - \mathbf{D}_{n_y} \mathbf{1} \right) \quad (2.69)$$

$$P_y^{(x)} = -r_x^T \left( \mathbf{S}^{-1} \mathbf{P}^\Gamma r_y - \mathbf{D}_{n_y} \mathbf{1} \right), \quad (2.70)$$

$$\Pi_0^{(x)} = -\frac{1}{2} \left( r_x^T \mathbf{D}_{r_x} + r_y^T \mathbf{D}_{r_y} \right) \left( \mathbf{S}^{-1} \mathbf{P}^\Gamma r_y - \mathbf{D}_{n_y} \mathbf{1} \right). \quad (2.71)$$

Thus, the components of the added mass coefficients tensor associated with translation in the  $x$  direction are

$$m_{xx}^F = \rho P_x^{(x)} \quad (2.72)$$

$$m_{xy}^F = \rho P_y^{(x)}, \quad (2.73)$$

$$m_x^M = \rho \left( \Pi_0^{(x)} - \mathbf{X}_c \times \mathbf{P}^{(x)} \right), \quad (2.74)$$

where  $\mathbf{X}_c$  is the centroid of the body, which can be calculated using (B 9), and the superscript  $F$  and  $M$  are used to denote the coefficient for the force and moment, respectively.

A similar approach can be used to obtain the added mass coefficients due to unit translation in the  $y$  direction, for which  $v_{b,x} = 0$ ,  $v_{b,y} = 1$ , and  $s'_b = -r_x$ . The coefficients due to unit rotation follow from taking  $v_{b,x} = -r_y$ ,  $v_{b,y} = r_x$ , and  $s'_b = -\frac{1}{2} (\mathbf{D}_{r_x} r_x + \mathbf{D}_{r_y} r_y)$ .

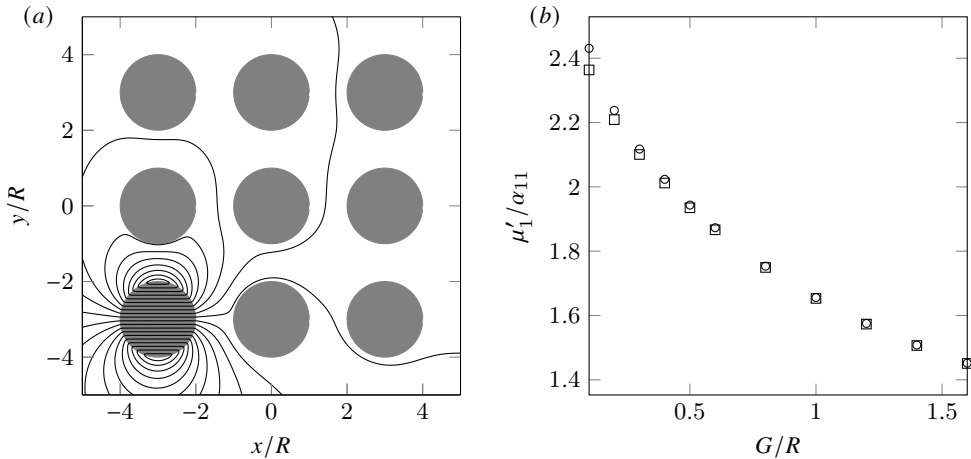


FIGURE 12. (a) Contours of the discrete streamfunction for an array of nine circular cylinders with radius  $R$ , spaced with a gap distance  $G$  between each cylinder, of which the bottom left cylinder translates horizontally. (b) Numerically simulated variation ( $\circ$ ) of the ratio between the principal value of added mass coefficient tensor and the largest self-added mass coefficient with the gap-to-radius ratio  $G/R$ . Overlaid are the values ( $\square$ ) obtained by [Chen \(1975\)](#) from solving a system of truncated analytical expressions. The simulations are performed with  $\Delta x/R = 0.05$  and  $\delta S/\Delta x = 2$ .

### 2.7. Multiple bodies

The previous sections provided the formulations for potential flow with the presence of a body. The extension of these expressions to multiple bodies is straightforward and consists of allocating partitions of  $f$  to the different bodies. The surface streamfunction has to be partitioned accordingly, with the body motion streamfunction  $s_b$  containing the values for the discrete surface points from all the bodies and  $s_0$  allocating a uniform value to each body. The system (2.12) can then be solved for the streamfunction field without modification.

If we want to enforce an edge condition on one or multiple bodies, each body with edge conditions has to add a Lagrange multiplier to the system. To accommodate the changes, we redefine  $s_0$  as a vector, containing these Lagrange multipliers and redefine  $I$  as a matrix with the  $(i, j)$ th entry equal to one if  $i$  is an index of  $f$  that belongs to the  $j$ th body with edge constraints and zero otherwise. With these new definitions, the saddle-point systems (2.29), (2.43), and (2.52) can be reused without further modification.

Figure 12 demonstrates an example of a potential flow model with an array of nine circular cylinders and compares the ratio of the principal value of added mass coefficient tensor and the largest self-added mass coefficient of the system with the results of [Chen \(1975\)](#).

## 3. Conclusion

We presented a two-dimensional, grid-based potential flow solver for use in a point vortex model to simulate a steady or unsteady, unbounded flow around a body, with possible edge conditions. In the development of this solver, we made use of two algebraic techniques that allow us to mimic the analytical treatment of potential flows around sharp-edged bodies. The first technique is to follow the immersed boundary projection method and introduce a Lagrange multiplier for the no-penetration constraint in the streamfunction Poisson equation, thus forming a saddle-point system. We can then identify the Lagrange multiplier as a discrete version of the continuous strength distribution of a bound vortex sheet on the body, a singular vorticity distribution that is commonly used to represent bodies in analytical potential flow. The second algebraic technique is

to decompose this discrete bound vortex sheet strength for sharp-edged bodies into a singular and smooth part. We can then add constraints on the elements of the smooth part that are located at the edges to make the overall discrete bound vortex sheet well-behaved. This allows us to enforce the Kutta condition in a way that is similar to analytical treatments of the Kutta condition and to introduce a way of enforcing generalized edge conditions. In a steady flow, one such constraint can be enforced at a time by adding it to the saddle point system. The Lagrange multiplier is then the—previously arbitrary—uniform value that can be added to the surface streamfunction. In an unsteady flow, where new point vortices can be introduced in the flow, we can enforce constraints on multiple edges. This requires adding the edge constraints and the constraint of zero total circulation to the saddle point system with their Lagrange multipliers being the uniform value of the surface streamfunction and the strengths of the new vortex elements. Furthermore, we can leverage the concept of the discrete bound vortex sheet strength to create expressions for the impulse in the flow around bodies and for the added mass matrix for a system of arbitrarily shaped bodies.

We found that our method can replicate the results of a Biot-Savart method for the unsteady flow around a flat plate with arbitrary precision. This motivates the goal of implementing a three-dimensional version of this solver since the concepts of the immersed boundary projection method and the enforcement of edge conditions through the multiplicative decomposition of the vortex sheet strength generalize to three dimensions. Such a three-dimensional, grid-based solver would rely on the vector potential and a vector treatment of the vorticity field, and it could potentially make significant cost improvements over similar three-dimensional Biot-Savart methods. It is also important to note that our method is only specific in its use of constrained forces for the immersed boundary projection method. The idea behind our method is not restricted to the discretization tools we used in our implementation.

## Acknowledgements

The support for this work by the US Air Force Office of Scientific Research (FA9550-18-1-0440) with programme manager Gregg Abate is gratefully acknowledged.

## Appendix A. Solution of general saddle-point systems

A general block system (with positive semi-definite matrix  $\mathcal{A}$ ) can be decomposed as follows:

$$\begin{bmatrix} \mathcal{A} & \mathcal{B}_1^T \\ \mathcal{B}_2 & -C \end{bmatrix} = \begin{bmatrix} \mathcal{A} & 0 \\ \mathcal{B}_2 & S \end{bmatrix} \begin{bmatrix} I & \mathcal{A}^{-1}\mathcal{B}_1^T \\ 0 & I \end{bmatrix}, \quad (\text{A } 1)$$

where

$$S \equiv -C - \mathcal{B}_2\mathcal{A}^{-1}\mathcal{B}_1^T \quad (\text{A } 2)$$

is the *Schur complement* of the matrix system and  $I$  is the identity. By this decomposition, we can develop an algorithm for the solution of the block system

$$\begin{bmatrix} \mathcal{A} & \mathcal{B}_1^T \\ \mathcal{B}_2 & -C \end{bmatrix} \begin{pmatrix} \mathbf{x} \\ \mathbf{y} \end{pmatrix} = \begin{pmatrix} \mathbf{r}_1 \\ \mathbf{r}_2 \end{pmatrix}. \quad (\text{A } 3)$$

We will refer to  $\mathbf{x}$  as the solution vector and  $\mathbf{y}$  as the constraint force. We define the intermediate solution vector  $(\mathbf{x}^*, \mathbf{y}^*)^T$  as the solution of the lower-triangular system

$$\begin{bmatrix} \mathcal{A} & 0 \\ \mathcal{B}_2 & S \end{bmatrix} \begin{pmatrix} \mathbf{x}^* \\ \mathbf{y}^* \end{pmatrix} = \begin{pmatrix} \mathbf{r}_1 \\ \mathbf{r}_2 \end{pmatrix} \quad (\text{A } 4)$$

and then the solution we seek can be found by back substitution of

$$\begin{bmatrix} 1 & \mathcal{A}^{-1}\mathcal{B}_1^T \\ 0 & 1 \end{bmatrix} \begin{pmatrix} \mathbf{x} \\ \mathbf{y} \end{pmatrix} = \begin{pmatrix} \mathbf{x}^* \\ \mathbf{y}^* \end{pmatrix} \quad (\text{A } 5)$$

The algorithm we derive from this is

$$\begin{aligned} \mathcal{A}\mathbf{x}^* &= \mathbf{r}_1, \\ \mathcal{S}\mathbf{y}^* &= \mathbf{r}_2 - \mathcal{B}_2\mathbf{x}^*, \\ \mathbf{y} &= \mathbf{y}^*, \\ \mathbf{x} &= \mathbf{x}^* - \mathcal{A}^{-1}\mathcal{B}_1^T\mathbf{y}. \end{aligned} \quad (\text{A } 6)$$

It is also useful to have an inverse representation of the block matrix system:

$$\begin{pmatrix} \mathbf{x} \\ \mathbf{y} \end{pmatrix} = \begin{bmatrix} \mathcal{A}^{-1} + \mathcal{A}^{-1}\mathcal{B}_1^T\mathcal{S}^{-1}\mathcal{B}_2\mathcal{A}^{-1} & -\mathcal{A}^{-1}\mathcal{B}_1^T\mathcal{S}^{-1} \\ -\mathcal{S}^{-1}\mathcal{B}_2\mathcal{A}^{-1} & \mathcal{S}^{-1} \end{bmatrix} \begin{pmatrix} \mathbf{r}_1 \\ \mathbf{r}_2 \end{pmatrix}. \quad (\text{A } 7)$$

## Appendix B. Some geometric relations for discrete surfaces

Consider a closed surface  $\mathcal{S}_b$  with unit normal  $\mathbf{n}$ . We will recall some basic geometric relations here, and then provide some discrete versions of these relations based on the set of points with coordinates  $r_x, r_y$ , and normal components  $n_x$  and  $n_y$  (which, the reader will recall, contain the surface length or area of each segment or panel associated with the points).

The volume  $\mathcal{V}_b$  of the region enclosed by  $\mathcal{S}_b$  can be computed from the integral

$$\mathcal{V}_b = \frac{1}{n_d} \int_{\mathcal{S}_b} \mathbf{x} \cdot \mathbf{n} \, dS, \quad (\text{B } 1)$$

where  $n_d$  is the number of spatial dimensions (2 or 3). Using the notation above, the approximate form of this expression is

$$\mathcal{V}_b \approx \frac{1}{n_d} \sum_j r_j^T n_j, \quad (\text{B } 2)$$

where the sum is taken over the  $n_d$  components.

An alternative formula for the volume is

$$\mathcal{V}_b \mathbf{e}_j = -\frac{1}{n_d - 1} \int_{\mathcal{S}_b} \mathbf{x} \times (\mathbf{n} \times \mathbf{e}_j) \, dS. \quad (\text{B } 3)$$

The components of this integral can be written discretely as

$$\mathcal{V}_b \mathbf{e}_j \approx \frac{\mathbf{e}_j}{n_d - 1} \sum_{k \neq j} r_k^T n_k \quad (\text{B } 4)$$

And finally, a third alternative is

$$\mathcal{V}_b \mathbf{I} = \int_{\mathcal{S}_b} \mathbf{x} \mathbf{n} \, dS, \quad (\text{B } 5)$$

where  $\mathbf{I}$  is the identity. The discrete form of this is a diagonal matrix with  $r_x^T n_x, r_y^T n_y$ , and  $r_z^T n_z$  along the diagonal.

Thus, we can conclude that the volume of the body is approximately

$$\mathcal{V}_b \approx r_x^T n_x \approx r_y^T n_y \approx r_z^T n_z, \quad (\text{B } 6)$$

or any average of some combination of these.

The centroid of the body can be derived from the equation

$$\mathbf{X}_c \mathcal{V}_b = \frac{1}{2} \int_{S_b} \mathbf{x} \cdot \mathbf{x} \mathbf{n} \, dS, \quad (\text{B } 7)$$

$$\mathbf{X}_c \times \mathcal{V}_b \mathbf{e}_j = -\frac{1}{n_d} \int_{S_b} \mathbf{x} \times [\mathbf{x} \times (\mathbf{n} \times \mathbf{e}_j)] \, dS, \quad (\text{B } 8)$$

$$X_c \approx \frac{1}{2\mathcal{V}_b} \left( r_x^T D_{r_x} + r_y^T D_{r_y} \right) n_x, \quad Y_c \approx \frac{1}{2\mathcal{V}_b} \left( r_x^T D_{r_x} + r_y^T D_{r_y} \right) n_y \quad (\text{B } 9)$$

## REFERENCES

- BAKER, G. R. 1979 The ‘‘cloud in cell’’ technique applied to the roll up of vortex sheets. *Journal of Computational Physics* **31** (1), 76–95.
- BECKERS, D. & ELDREDGE, J. D. 2021 JuliaIBPM/GridPotentialFlow.jl v0.1.0. Available at: <https://github.com/JuliaIBPM/GridPotentialFlow.jl/tree/v0.1.0>.
- BENZI, M., GOLUB, G. H. & LIESEN, J. 2005 Numerical solution of saddle point problems. *Acta Numerica* **1**, 1–137.
- CHATELAIN, P., CURIONI, A., BERGDORF, M., ROSSINELLI, D., ANDREONI, W. & KOUMOUTSAKOS, P. 2008 Billion vortex particle direct numerical simulations of aircraft wakes. *Computer Methods in Applied Mechanics and Engineering* **197** (13–16), 1296–1304.
- CHATELIN, R. & PONCET, P. 2014 Hybrid grid-particle methods and Penalization: A Sherman-Morrison-Woodbury approach to compute 3D viscous flows using FFT. *Journal of Computational Physics* **269**, 314–328.
- CHEN, S. S. 1975 Vibration of nuclear fuel bundles. *Nuclear Engineering and Design* **35** (3), 399–422.
- CHORIN, A. J. & BERNARD, P. S. 1973 Discretization of a vortex sheet, with an example of roll-up. *Journal of Computational Physics* **13** (3), 423–429.
- CHRISTIANSEN, J.P. 1973 Numerical simulation of hydrodynamics by the method of point vortices. *Journal of Computational Physics* **13** (3), 363–379.
- COLONIUS, T. & TAIRA, K. 2008 A fast immersed boundary method using a nullspace approach and multi-domain far-field boundary conditions. *Computer Methods in Applied Mechanics and Engineering* **197** (25–28), 2131–2146.
- COQUERELLE, M. & COTTET, G.-H. 2008 A vortex level set method for the two-way coupling of an incompressible fluid with colliding rigid bodies. *Journal of Computational Physics* **227** (21), 9121–9137.
- COTTET, G.-H. & KOUMOUTSAKOS, P. 2000 *Vortex Methods: Theory and Practice*. Cambridge, UK: Cambridge University Press.
- COTTET, G.-H. & PONCET, P. 2004 Advances in direct numerical simulations of 3D wall-bounded flows by Vortex-in-Cell methods. *Journal of Computational Physics* **193** (1), 136–158.
- COUËT, B., BUNEMAN, O. & LEONARD, A. 1981 Simulation of three-dimensional incompressible flows with a vortex-in-cell method. *Journal of Computational Physics* **39** (2), 305–328.
- CSERTI, J. 2000 Application of the lattice green’s function for calculating the resistance of an infinite network of resistors. *Am. J. Phys* **68**, 896–906.
- DARAKANANDA, D. & ELDREDGE, J. D. 2019 A versatile taxonomy of low-dimensional vortex models for unsteady aerodynamics. *J. Fluid Mech.* **858**, 917–948.
- EBIANA, A.B. & BARTHOLOMEW, R.W. 1996 Design considerations for numerical filters used in Vortex-in-cell algorithms. *Computers & Fluids* **25** (1), 61–75.
- ELDREDGE, J. D. 2019 *Mathematical Modeling of Unsteady Inviscid Flows, Interdisciplinary Applied Mathematics*, vol. 50. Springer.
- GAZZOLA, M., CHATELAIN, P., VAN REES, W. M. & KOUMOUTSAKOS, P. 2011 Simulations of single and multiple swimmers with non-divergence free deforming geometries. *Journal of Computational Physics* **230** (19), 7093–7114.
- GILLIS, T., WINCKELMANS, G. & CHATELAIN, P. 2018 Fast immersed interface Poisson solver for 3D unbounded problems around arbitrary geometries. *Journal of Computational Physics* **354**, 403–416.

- HEJLESEN, M. M., KOUMOUTSAKOS, P., LEONARD, A. & WALTHER, J. H. 2015 Iterative Brinkman penalization for remeshed vortex methods. *Journal of Computational Physics* **280**, 547–562.
- KATSURA, S. & INAWASHIRO, S. 1971 Lattice Green's functions for the rectangular and the square lattices at arbitrary points. *J. Math. Phys.* **12**, 1622–1630.
- LEVEQUE, R.J. & LI, Z. 1994 The Immersed Interface Method for Elliptic Equations with Discontinuous Coefficients and Singular Sources. *SIAM Journal on Numerical Analysis* **31** (4), 1019–1044.
- LISKA, S. & COLONIUS, T. 2014 A parallel fast multipole method for elliptic difference equations. *J. Comput. Phys.* **278**, 76–91.
- MARICHAL, Y., CHATELAIN, P. & WINCKELMANS, G. 2014 An immersed interface solver for the 2-D unbounded Poisson equation and its application to potential flow. *Computers and Fluids* **96**, 76–86.
- MENG, J. C. S. & THOMSON, J. A. L. 1978 Numerical studies of some nonlinear hydrodynamic problems by discrete vortex element methods. *Journal of Fluid Mechanics* **84** (3), 433–453.
- MONAGHAN, J. J. 1985 Extrapolating B splines for interpolation. *Journal of Computational Physics* **60** (2), 253–262.
- PONCET, P. 2009 Analysis of an immersed boundary method for three-dimensional flows in vorticity formulation. *Journal of Computational Physics* **228** (19), 7268–7288.
- RAMESH, K., GOPALARATHNAM, A., GRANLUND, K., OL, M. V. & EDWARDS, J. R. 2014 Discrete-vortex method with novel shedding criterion for unsteady aerofoil flows with intermittent leading-edge vortex shedding. *J. Fluid Mech.* **751**, 500–548.
- RASMUSSEN, J. T., COTTET, G.-H. & WALTHER, J. H. 2011 A multiresolution remeshed Vortex-In-Cell algorithm using patches. *Journal of Computational Physics* **230** (17), 6742–6755.
- ROSSINELLI, D., BERGDORF, M., COTTET, G.-H. & KOUMOUTSAKOS, P. 2010 GPU accelerated simulations of bluff body flows using vortex particle methods. *Journal of Computational Physics* **229** (9), 3316–3333.
- SPIETZ, H. J., HEJLESEN, M. M. & WALTHER, J. H. 2017 Iterative Brinkman penalization for simulation of impulsively started flow past a sphere and a circular disc. *Journal of Computational Physics* **336**, 261–274.
- WIEGMANN, ANDREAS & BUBE, KENNETH P 2000 The Explicit-Jump Immersed Interface Method: Finite Difference Methods for PDEs with Piecewise Smooth Solutions. *SIAM Journal on Numerical Analysis* **37** (3), 827–862.